NeuroImage: Clinical 28 (2020) 102442

Contents lists available at ScienceDirect

NeuroImage: Clinical

journal homepage: www.elsevier.com/locate/ynicl

The bed nucleus of the stria terminalis and functionally linked neurocircuitry modulate emotion processing and HPA axis dysfunction in posttraumatic stress disorder

Samir Awasthi[a], Hong Pan[a], Joseph E. LeDoux[c], Marylene Cloitre[d,e], Margaret Altemus[f], Bruce McEwen[g], David Silbersweig[a,*], Emily Stern[a,b]

[a] Department of Psychiatry, Brigham and Women's Hospital, Harvard Medical School, Boston, MA, USA
[b] Department of Radiology, Brigham and Women's Hospital, Harvard Medical School, Boston, MA, USA
[c] Center for Neural Science, New York University, New York, NY, USA
[d] National Center for PTSD, Veteran Affairs Palo Alto Health Care System, USA
[e] Department of Psychiatry and Behavioral Sciences, Stanford University, Palo Alto, CA, USA
[f] Department of Psychiatry, Yale School of Medicine, New Haven, CT, USA
[g] Rockefeller University, New York, NY, USA

ARTICLE INFO

Keywords:
Bed nucleus of the stria terminalis
PTSD
fMRI
Functional connectivity
Hypothalamic pituitary adrenal (HPA) axis
Subcortical brain networks

ABSTRACT

Background: The bed nucleus of the stria terminalis (BNST) plays an important role in rodent posttraumatic stress disorder (PTSD), but evidence to support its relevance to human PTSD is limited. We sought to understand the role of the BNST in human PTSD via fMRI, behavioral, and physiological measurements.
Methods: 29 patients with PTSD (childhood sexual abuse) and 23 healthy controls (HC) underwent BOLD imaging with an emotional word paradigm. Symptom severity was assessed using the Clinician-Administered PTSD Scale and HPA-axis dysfunction was assessed by measuring the diurnal cortisol amplitude index (DCAI). A data-driven multivariate analysis was used to determine BNST task-based functional co-occurrence (tbFC) across individuals.
Results: In the trauma-versus-neutral word contrast, patients showed increased activation compared to HC in the BNST, medial prefrontal cortex (mPFC), posterior cingulate gyrus (PCG), caudate heads, and midbrain, and decreased activation in dorsolateral prefrontal cortex (DLPFC). Symptom severity positively correlated with activity in the BNST, caudate head, amygdala, hippocampus, dorsal anterior cingulate gyrus (dACG), and PCG, and negatively with activity in the medial orbiotofrontal cortex (mOFC) and DLPFC. Patients and HC showed marked differences in the relationship between the DCAI and BOLD activity in the BNST, septal nuclei, dACG, and PCG. Patients showed stronger tbFC between the BNST and closely linked limbic and subcortical regions, and a loss of negative tbFC between the BNST and DLPFC.
Conclusions: Based upon novel data, we present a new model of dysexecutive emotion processing and HPA-axis dysfunction in human PTSD that incorporates the role of the BNST and functionally linked neurocircuitry.

1. Introduction

Post-traumatic stress disorder (PTSD) is a heterogeneous condition that is characterized by symptoms of intrusion, avoidance, negative cognitions or mood, and hyperarousal (Longo et al., 2017). The disorder involves abnormalities in multiple functional domains, including threat detection, assessment, learning and unlearning, emotion regulation, and executive function (Ross et al., 2017; Pitman et al., 2012). Neuroanatomical investigations into the corresponding neural substrates have most consistently revealed lower gray matter volumes in the hippocampus, ventromedial prefrontal cortex (vmPFC), and dorsal anterior cingulate gyrus (dACG) in PTSD subjects compared to healthy controls (HC) (Ross et al., 2017; Pitman et al., 2012). Similarly, studies utilizing task-based functional neuroimaging involving trauma-, threat-, fear-, or negative emotion-based tasks have most frequently found hyperactivity in the amygdala and dACG and hypoactivity in the medial prefrontal cortex (mPFC) (Ross et al., 2017; Pitman et al., 2012), though conflicting reports exist in the literature. These results, in

* Corresponding author at: Department of Psychiatry, Brigham and Women's Hospital, 60 Fenwood Rd, Boston, MA 02115, USA
E-mail address: dsilbersweig@bwh.harvard.edu (D. Silbersweig).

https://doi.org/10.1016/j.nicl.2020.102442
Received 8 April 2020; Received in revised form 14 September 2020; Accepted 15 September 2020
Available online 24 September 2020

conjunction with complementary rodent studies, have led to the development of a model for PTSD in which dysfunctional mPFC-mediated regulation of the amygdala plays a central role in the production of behavioral symptoms (Etkin et al., 2011). While this model captures important aspects of PTSD, several studies in rodent models of PTSD also point towards the importance of the bed nucleus of the stria terminalis (BNST) in the genesis and pathophysiology of the disorder (Lebow and Chen, 2016).

The BNST is a complex, sexually dimorphic, subcortical nucleus located in the basal forebrain. In animal studies it has been implicated in threat processing and risk assessment (LeDoux and Pine, 2016), anxiety (Adhikari, 2014; Grupe and Nitschke, 2013), rewarding and aversive motivational states (Jennings et al., 2013), and PTSD-like-behavior (Elharrar et al., 2013; Henckens et al., 2017; Lebow et al., 2012), yet only preliminary evidence links it to human PTSD (Brinkmann et al., 2017). In both rodents and humans, the BNST has prominent white matter connectivity with the amygdala via the stria terminalis, as well as with the inferior hippocampus, hypothalamus, thalamus, and infralimbic/ventromedial prefrontal cortex (vmPFC) (Lebow and Chen, 2016; Avery et al., 2014). Anatomic connectivity to dopaminergic, serotoninergic, and noradrenergic nuclei in the brainstem has also been demonstrated in rodents. Immunohistochemical studies have shown that the BNST contains a high density of neuroendocrine receptors for key stress-responsive neuropeptides including corticotropin-releasing factor (CRF) (Elharrar et al., 2013; Asok et al., 2018; Hammack et al., 2010), vasopressin, and pituitary adenylate cyclase-activating polypeptide type 1 (PACAP1) (Goode and Maren, 2017). It is therefore uniquely situated to integrate and mediate emotion processing and the corresponding physiological expressions in a context-dependent manner (Lebow and Chen, 2016). Animal studies have implicated the region in defensive responses to sustained or unpredictable threat (Rodríguez-Sierra et al., 2016) and have further demonstrated that it is hyperactive in these contexts in models of PTSD (Lebow et al., 2012; Somerville et al., 2010). In humans, investigators have used task-based blood-oxygen-level-dependent (BOLD) fMRI to demonstrate that the BNST is involved in threat monitoring (Herrmann et al., 2016) and threat anticipation (Davis et al., 2010). Moreover, it is hyperactive in these paradigms, respectively, in individuals with high trait anxiety and PTSD (Brinkmann et al., 2017; Herrmann et al., 2016). Studies aimed at differentiating the role of the BNST from that of the amygdala suggest that the amygdala differentially activates to immediate threat whereas the BNST differentially activates to sustained or unpredictable threat (Davis et al., 2010; Klumpers et al., 2017). In one human study, a discernable shift in BOLD activity from the BNST to the amygdala was observed as shock anticipation shifted to shock confrontation (Weisholtz et al., 2015). The contextual dissociation discussed here, though controversial, suggests that the BNST may play an important role in threat processing, specifically in the sustained hypervigilance and hyperarousal characteristic of PTSD. However, the disorder affects several behavioral domains independently of an objectively threatening context, and these functions might also be modulated by the BNST (Lebow and Chen, 2016). There is therefore a need to understand the role of the BNST in the broader pathophysiology of human PTSD.

In the present work, we investigate the neurobiology of PTSD with a focus on the BNST as a key component of whole brain networks underlying the disorder by performing a exploratory analysis on existing data. In order to gain a more comprehensive, multi-dimensional understanding of the neurocircuitry involved, we combine task-based fMRI with behavioral data, physiological data, and a multivariate analysis of task-based functional co-occurrence (tbFC). We use an emotional word paradigm (Isenberg et al., 1999; First and Gibbon, 2004) specifically tailored to trauma-related content to examine BNST activity, and interpret the results in the context of whole brain activity and correlations of the BOLD signal to PTSD symptom severity and diurnal cortisol amplitude index (DCAI). Based on previous BNST research discussed above and on the absence of a direct threat in the emotional word paradigm, we hypothesized that the BNST would be increased during the processing of trauma-related vs. neutral words in PTSD patients when compared to healthy controls. We incorporate our results with the existing literature in order to present a more comprehensive model for altered BNST function in PTSD.

2. Material and methods

2.1. Study participants

Individuals were recruited via community-based advertisements in New York City, NY, USA in non-clinical settings. Study participants consisted of 29 sexual assault victims who met DSM-IV criteria for PTSD (25 females, mean age = 34.6, SD = 9.2 years, range = 20–55), and 23 healthy control subjects (11 females, mean age = 28.7 (SD = 7.6) years, range = 20–48). All participants experienced trauma at age 21 or younger and the mean time elapsed since trauma as of the scanning day was 24.6 years (SD 10.3, range 1–42). All participants were right-handed, native English speakers, and were free of other psychiatric diagnoses, substance abuse, and significant neurological or medical disorders such as head trauma, stroke, diabetes mellitus, or cardiovascular disease. In addition, urine toxicology was performed prior to scanning. All subjects were free of psychotropic medications for at least 1 year prior to scanning. All subjects were characterized using the Structured Clinical Interview for DSM-IV I (SCID I) (Beck et al., 1961) criteria, Beck Depression Inventory (Spielberger, 1983), State-Trait Anxiety Inventory (WIENER, 1992), Dissociative Experience Scale (Spielberger, 1999). PTSD subjects were additionally characterized using the Structured Clinical Interview for DSM-IV Personality Disorders (SCID-II) (Beck et al., 1961), State Trait Anger Expression Inventory (Foa et al., 1997), PTSD Symptom Scale-Self Report (Carver et al., 1989), COPE (Reiss et al., 1986), and Anxiety Sensitivity Index (Blake et al., 1995). Trauma history was assessed using the Sexual Assault and Adult Interpersonal Violence and Childhood Interpersonal Violence Before Age 18 scales. The diagnosis of PTSD was established using the Clinician Administered PTSD Scale (CAPS) (Macmillan and Creelman, 2005). CAPS scores available for 27 out of 29 patients and ranged from 33 to 102 with a mean of 61.62 (SD = 17.03). All participants gave informed consent prior to participation in the study, which was part of a protocol approved by the Institutional Review Board at New York-Presbyterian Hospital/Weill Medical College of Cornell University. A continuing analysis of the data was approved by the Institutional Review Board at Brigham and Women's Hospital.

2.2. Cortisol sample collection and analysis

Salivary cortisol samples were collected using cotton swabs (Sarstedt, Newton, NC). Subjects were instructed to place the cotton swab in their mouths for approximately 2 min until saliva had accumulated in the cotton. The swab was then placed inside of a plastic tube for storage. Eight cortisol samples were collected during a normal day. Subjects were asked to collect saliva immediately upon waking (WU), 30 min and 60 min following their wake up (WU + 30, WU + 60), and at 1100 h, 1400 h, 1700 h, 2000 h and 2300 h later that day. Subjects recorded the actual time that they took the sample. Saliva samples were then stored at − 70 °C prior to analysis. Cortisol was measured using one of two assays: 1) a commercial ELISA assay optimized for salivary samples (Salimetrics LLC, State College, Pennsylvania, USA), performed by a research laboratory at Weill/Cornell Medical Center, or 2) A solid phase radioimmunoassay, using test tubes pre-coated with antibody specific for cortisol and I^{125} labeled cortisol-3-derivative as a ligand (Micromedic RIA kit: Micromedic Systems, Inc., Subsidiary of Rohm and Haas Co., Horsham, PA). The latter assay was discontinued during the study. All analysis of cortisol were conducted with Instrument Type as a covariate of no interest in order to account for the potential impact of assay type on the results. Additionally, all samples were assayed in

duplicate in the same assay. All samples were run in duplicate and the mean value was used for analysis. A diurnal cortisol amplitude index (DCAI) was generated with the following equation:

$$\frac{Max(WU,\ WU+30,\ WU+60) - Average(2000h,\ 2300h)}{Max(WU,\ WU+30,\ WU+60) + Average(2000h,\ 2300h)}$$

$Max(WU,\ WU+30,\ WU+60)$represents the maximum cortisol value among the WU, WU + 30 and WU + 60 samples during a day, and $Average(2000h,\ 2300h)$ signifies the average of the last two cortisol samples taken for the day. This index reflects the daily excursion of cortisol level over a normal day, and is sensitive to both a high wake up value and/or a low evening value. This diurnal cortisol amplitude index was entered as the covariate of interest in image correlation analysis. The mean cortisol level for a normal day was calculated as $verage(1100h,\ 1400h,\ 1700h,\ 2000h,\ 2300h)$. Complete cortisol measures were available for 21 (10 females) of 23 healthy control subjects, and 11 (8 females) of 29 PTSD patients (some participants did not complete a full day of sample collection).

2.3. Task-based fMRI Experiment: Emotional word paradigm

Stimuli consisted of 48 negative/anxiety (24 negative/PTSD, 24 negative/panic), 48 neutral, and 48 positive/safety words, balanced across categories for frequency, length, and part of speech (nouns and adjectives/verbs). Posttraumatic stress disorder words were designed to be relevant to physical/sexual trauma; panic words were designed to be relevant to panic attack symptoms and somatic/illness-related anxiety (a negative control condition, as well as explicit probes for panic disorder patients also studied as part of a larger project); and positive words were designed to be counter-anxiety and evocative of safety, relaxation, and reward, as defined by the literature and clinical experience. These word types were rated for suitability by a panel of three experienced clinicians. They were a subset of a list of words that had been piloted on 34 normal subjects, who rated the three word types (positive, negative, and neutral) as significantly different in valence ($p < 0.001$) and rated positive and negative words as not significantly different in intensity ($p > 0.2$). Examples are as follows: negative/PTSD–rape, assault, force; negative/panic–frantic, death, cancer; neutral–bookcase, clarinet, rotate; positive/rewarding–safe, gentle, delighted.

The three valences of words were presented within a block design (six words per block, eight blocks per valence), with blocks balanced to control for order and time effects (SI Fig. 1). Posttraumatic stress disorder words and panic words were presented for four blocks each (each representing half of the total negative word blocks). Each word appeared for 2 s, followed by an inter-stimulus interval jittered around an average of 2.8 s, for a total of 28.8 s per block. Blocks were presented in four study epochs containing six blocks each. Each block was followed by 24 s of rest, with each epoch as a whole preceded and followed by 2 additional 12-second rest periods. The entire word paradigm took approximately 24 min. During presentation of stimuli, subjects were instructed to read each word silently and to then immediately press a button under their right index finger. During rest periods, they were instructed to look at a dash at the center of the screen and to have their minds either blank or floating freely.

After the emotional word paradigm, subjects were removed from the scanner and given an incidental memory test utilizing a list of words consisting of the 144 stimuli seen during scanning (targets) randomly interspersed with 72 other words (distracters to control for false alarms); divided equally into negative (PTSD and panic), neutral, and positive categories; and balanced for the same qualities as the targets. They were instructed to read each word and to indicate those that they believed they had seen in the scanner. Following completion of that task, subjects were also asked to rate the valence of each word on a 7-point Likert-like scale (–3 = very negative, 0 = neutral, +3 = very positive).

2.4. Behavioral analyses

Recognition memory performance was evaluated with discrimination index d' based on Signal Detection Theory (Protopopescu et al., 2005). ANCOVA was employed to test for Group and Word Category effects on in-scanner button-press response time, post-scan word recognition rate, word valence rating scale, and word intensity. Word intensity was defined as the absolute difference between the valence ratings of a valenced and neutral word type (Gu et al., 2002) with Age and Sex as covariates. Subsequent t-tests were used to explore within-group effects.

2.5. fMRI image acquisition

Images were acquired with a research-dedicated GE Signa 3 Tesla MRI scanner (max gradient strength 40mT/m; max slew rate 150 T/m/s) (General Electric Company, Waukesha, Wisconsin) with an MRI-compatible head holder at the Weill Medical College of Cornell University. Anatomical localization: Three to five T1 weighted sagittal slices were collected to localize the anterior and posterior commissures, followed by a set of 17 coronal slices perpendicular to the AC-PC line to determine the location of the amygdala and hippocampus. A reference T1 weighted anatomical image with the same axial slice placement and thickness as the functional imaging was then acquired with two slices centered within the amygdala, as the proxy for co-registration purpose (256x256 matrix size, 5 mm in thickness, 1 mm gap, TE/TR = 14/500 ms, FoV = 240 mm). Functional imaging: Blood Oxygenation Level-Dependent (BOLD) contrast imaging, which reflects changes in venous deoxyhemoglobin associated with neuronal activity, was employed. After shimming to maximize homogeneity, a series of functional scans was collected using a gradient echo EPI sequence (TR = 1200 ms, TE = 30 ms, 15 or 21 slices of 5 mm in thickness, 1 mm gap, FoV = 240 mm, matrix = 64x64), with a z-shimming algorithm (Friston, 2007) to reduce susceptibility-induced signal losses at the base of the brain. Structural imaging: A high-resolution T1 weighted anatomical image was acquired using a spoiled gradient (SPGR) recalled acquisition sequence (TR/TE = 30/8msec, flip angle = 45, field of view = 220 mm, 140 coronal slices with thickness = contiguous 1.5 mm, number of averages = 1, matrix = 256x256, voxel resolution = 0.8594x1.5x0.8594 mm^3). Functional MRI System: The Integrated Functional Imaging System SA/E-Prime environment (IFIS-SA, MRI Devices, Waukesha WI; Psychology Software Tools, Pittsburgh PA) were configured and programmed for visual and auditory stimulus delivery and response collection (via the head coil-mounted LCD display, headphones and Brainlogics Fiber Optic Button Response Units) that were synchronized via MRI scanner trigger signal in the MRI scanning protocol.

2.6. fMRI image processing

The functional image processing pipeline consists of the following steps using customized SPM software (Pan et al., 2011; Frank et al., 2001): Reconstruction of EPI functional images using modified GE reconstruction software with off-resonance phase correction, slice-timing correction and Hanning-window apodization; Extraction of physiological fluctuations such as cardiac and respiratory cycles from EPI image sequence (Worsley et al., 2002); Manual AC-PC re-orientation of the two anatomical images and application of the transformation parameters of the reference T1 image to all functional EPI-BOLD images; Realignment to further correct for slight head movement between scans and for differential spin excitation history based on intracranial voxels; Co-registration of functional EPI-BOLD images to the corresponding high-resolution T1 anatomical image, based on the rigid body transformation parameters of the reference T1 image to the high-resolution

T1 anatomical image for each individual subject; Stereotactic normalization to a standardized coordinate space (Montreal MRI Atlas version of Talairach space) based on the high-resolution T1 anatomical image to normalize for individual differences in brain morphology (12 nonlinear iterations, 7 × 8 × 7 nonlinear basis functions, medium regularization, and resampled to 3 × 3 × 3 mm^3 voxels using sinc interpolation), and application of the normalization transformation to all functional EPI-BOLD images; Spatial smoothing of all the normalized functional EPI-BOLD images with an isotropic Gaussian kernel (FWHM = 7.5 mm). Extensive examination of processed images at each intermediate stage for quality assurance was performed both by visual inspection and quantitation. fMRI data sets in this study were quality controlled against and met with the stringent criteria that there is no movement of > 1/3 voxel over the study session for each participant.

2.7. Univariate functional image analysis

Using customized fmristat software (Aguirre et al., 1998), a two-level voxel-wise linear mixed-effects model was utilized to examine the effect sizes of the key Group/Condition contrasts in an ANCOVA setting. First, a voxel-wise multiple linear regression model was employed at the individual subject level. This comprised of the block-by-block regressors of interest, which consist of the each stimulus block onset time/duration convolved with a prototypical hemodynamic response function, and the covariates of no interest, which consist of the temporal first-order derivative of the principal regressors (to compensate slight latency differences in individual hemodynamic response from the prototypical response function), global fluctuations, physiological fluctuations, realignment parameters, and scanning periods (McGonigle et al., 2000; Theiss et al., 2017). Temporal filtering was performed to counter the effects of baseline shifts and higher frequency noise, and a voxel-wise *AR(1)* model of the time course was used to accommodate temporal correlation in consecutive scans. Effects at every brain voxel were estimated using the EM (expectation maximization) algorithm, and task-specific condition effects of Word Type were then compared using linear contrasts. Second, at the group level, a mixed-effects model (with the Subject factor as the random-effect) was used. The within- and between-group effects of the hypothesis-driven contrast (the hypothesis-driven contrast is PTSD Words vs Neutral Words : PTSD Group vs HC Group) was then estimated using an EM algorithm, with demographic variables (age, sex) incorporated as covariates of no interest. The within-group correlation analyses of the hypothesis-driven contrasts with clinic and physiological measures (CAPS and diurnal cortisol amplitude) was also performed at the group level with mixed-effects models. These group-level effect estimates generate statistical maps of the *t*-statistic, and the statistical significance of the *t*-maps was then evaluated in the final step of inference. The statistical inference was based on random field theory, where the statistical parametric map of each contrast was thresholded and the cluster sizes were reported at an initial voxel-wise p-value < 0.01 with cluster spatial extent > 250 mm^3, and the p-values at the peak voxels were corrected for multiple comparisons based on family-wise error rate over the whole brain or within a priori Regions of Interest (ROIs) at $p_{corrected} < 0.05$. For identification of the BNST, the probabilistic mask of Theiss et al. (Craddock et al., 2012); thresholded at > 0 (total volume of BNST = 354 mm^3) was used (SI Fig. 2).

2.8. Multivariate functional image analysis

To compute task-based functional co-occurrence (tbFC), a we used a customized algorithmic pipeline based on a previously validated analytic approach that has been shown to better reproduce voxel-level connectivity compared to the anatomic atlas-based computation of functional connectivity (Shi and Malik, 2000). The algorithm was implemented at the group level and consisted of the following computational components:

(A) An automated functional localizome mapping (brain region parcellation) algorithm, utilizing a normalized spectral clustering method (Foley and Kirschbaum, 2010), used task/condition-specific effect size images as inputs, to generate a set of task-condition-specific functional brain region parcellations with a pre-specified range of region numbers (from 100 to 3000 parcellation regions, with increments of 100). The brain region is constrained by a searching space, a shared brain mask image defined via an algorithm that utilizes both anatomical image and functional image of each individual from the group of 29 PTSD subjects in this study. For generating this particular set of functional localizome maps, each subject contributes two condition-specific effect size images (corresponding to the two conditions: “PTSD Word” and “Neutral Word” in Emotional Word Paradigm; for the group of 29 PTSD subjects there will be 58 such images used as inputs in the parcellation algorithm). The 30 resulting sets of task-condition-specific brain region parcellation map with the pre-specified range of region numbers, span a space for defining a set of spatially distinct functional regions/nodes.

(B) An automated selection and sorting algorithm was used to define the stereotactic coordinate representing each parcellated brain region in the following steps: For each parcellated region, the coordinate with the highest absolute t-statistic value of the contrast of interest (“PTSD Word vs Neutral Word” in Emotional Word Paradigm) at the group level is chosen to represent that region. Since both BNST and Septal Nuclei are the hypothesized ROIs of this study, and there are five candidate coordinates at (9, 6, −3), (6, 3, 6), (-6, 3, 3), (3, 6, 3) and (3, 9, −6) in five candidate parcellated regions representing the BNST (the first three coordinates) and Septal Nuclei (the last two coordinates) respectively in the set of brain region parcellation map with the pre-specified region number at 2300 (more than the rest of other parcellation maps which only contain two out of the five candidates at the most), this particular set of brain region parcellation map where both ROIs are represented is chosen. This results in a final parcellation map of 1764 non-empty regions/nodes represented by their respective stereotactic coordinates, to be used in subsequent multivariate statistical analyses of functional co-occurrence.

(C) Thresholding correlation analyses within PTSD patient group and healthy control group, are performed by calculating the group-level inter-regional correlation matrix based on the effect size images of the contrast of interest (“PTSD Word vs Neutral Word” in Emotional Word Paradigm) at 1764 representative coordinates of the functional parcellation map. The resulting group-level task-based functional co-occurrence (tbFC) measures (correlation with BNST) are then thresholded at $p < 0.01$, and reported in Supplemental Table 4.

3. Results

3.1. Reaction times

Within either PTSD patient group or HC group, there was no significant difference in reaction time across word categories. PTSD subjects had slower overall reaction times (Mean = 904.67 ms, SD = 275.06 ms) than HC (Mean = 816.02 ms, SD = 263.95 ms) (p = 0.0231), but the effect did not depend on word category, age, sex, or interaction terms among these factors.

3.2. Recognition memory

Recognition memory performance was evaluated with discrimination index d’ based on Signal Detection Theory (Protopopescu et al., 2005). Across groups, there was no difference in performance, though there were effects of word category [F(3,189) = 5.248, p = 0.00168] and sex [F(1,189) = 4,512, p = 0.03495] that are explained by the

following within-group effects. Within the PTSD group, there was a significant effect in word categories (p = 0.0097) that did not depend on age, sex, or any interaction terms. PTSD words (d' = 1.7334) were recognized at significantly higher rates than panic words [t(55.847) = 1.7626, p = 0.039; d' = 1.3348], neutral words [t(52.513) = 2.845, p = 0.0032; d' = 1.1558], and positive words [t(55.525) = 3.0959, p = 0.0015; d' = 0.9935]. Within the group of healthy subjects, there were no significant differences in recognition memory performance among word types, though there was a sex effect with higher recognition memory in females (p = 0.002, d' = 1.5422 for females, and 1.0356 for males).

3.3. Valence ratings

Word valence was assessed using a 7-point Likert-like scale (-3 = very negative, 0 = neutral, +3 = very positive). Across groups, there were significant Group [F(1,187) = 12.219, p = 0.000591] and Word Category effects [F(3,187) = 455.976, p < 2e-16]. The PTSD patient group rated each word type with lower average valence than the HC group. When the Group effects were examined per Word Category, significant Group effects were observed in the PTSD [t(41.484) = 2.294, p = 0.0133] and Positive [t(46.679) = 2.0015, p = 0.0256] word types, while there was no significant difference in valence rating for neutral words (p = 0.0847) or panic words (p = 0.3072). The PTSD word type was rated significantly lower than the panic word type [t(25) = 4.0986, p = 0.0002; 0.304 lower on average) within the PTSD patient group, whereas it was rated marginally lower [t(22) = 1.7606, p = 0.0461; 0.101 lower on average] in the HC group. Both groups rated the three word types (negative, neutral, and positive) as significantly different in valence (p < 0.0001), but the PTSD patient group rated negative words significantly higher in intensity than positive words (p = 0.0015; 0.4964 higher in intensity) whereas the HC group rated negative and positive words as not significantly different in intensity (p = 0.1023).

3.4. Diurnal cortisol amplitude index

The effect of PTSD diagnosis on the DCAI and mean cortisol levels was determined by ANCOVA, with Age, Sex and Instrument Type as covariates. There was a significant effect at the group level [F(1,29) = 12.65, p < 0.00131] and a post hoc *t*-test revealed that this group difference in DCAI was caused by the HC group showed having a higher amplitude of the DCAI (Mean = 0.5424, SD = 0.2400) than the PTSD patient group (Mean = 0.2549, SD = 0.3022) [t(19) = 2.8259, p = 0.0054]. ANCOVA of the mean cortisol level showed no factor(s) and interaction(s) that were significantly different between the two groups [F(1,24) = 0.758, p = 0.393] [PTSD mean = 0.5447 μg/dL (SD = 0.3396 μg/dL), HC mean = 0.4491 μg/dL (SD = 0.2764 μg/dL)].

3.5. fMRI findings in the trauma versus neutral word contrast

We investigated the hypothesis that BNST activity is elevated in PTSD relative to HC during the processing of trauma-related words. In the between-group trauma-versus-neutral word contrast, patients showed increased activation compared to HC in the BNST, mPFC, posterior cingulate gyrus (PCG), caudate heads, and midbrain, and decreased activation in dorsolateral prefrontal cortex (DLPFC). Within- and between-group results in the trauma versus neutral word are summarized in Table 1 and Fig. 1, with condition-specific effect sizes displayed in Fig. 1D-N and extended results in Supplementary Table 1.

3.6. Correlations of task-based activation with symptom severity

In PTSD patients, symptom severity (CAPS score) positively correlated with activity in the trauma-versus-neutral word contrast of the BNST, caudate head, amygdala, hippocampus, dACG, and PCG, and negatively with activity in the medial OFC and DLPFC (Table 1, Fig. 2, extended results in Supplementary Table 2). Between-group comparisons of these correlations were not performed.

3.7. Correlations of task-based activation to HPA axis dysfunction

We examined correlations of the DCAI to BOLD activity in the trauma-versus-neutral word contrast during the early phase of the task, defined as the first half of the emotional word paradigm (Fig. 3, Supplementary Table 3). The early phase was used so the findings more likely reflected associations of BOLD activity with the typical DCAI. BOLD activity later in the scanning session may be associated with an acute stress response and cortisol release, and less likely to correspond to diurnal cortisol measures obtained on a different day. Serum cortisol levels begin to rise within minutes of onset of an acute stressor and peak 10–30 min after stressor onset (Lovallo et al., 2010). Indeed, Protopopescu et al. (Gu et al., 2002) have previously shown that amygdala activity is higher in the early portion of the emotional word paradigm, while others have demonstrated that acute administration of a corticosteroid reduces limbic BOLD activity (Garcia-Garcia et al., 2018). In PTSD, negative correlations were identified in the right PCG, middle temporal gyrus (MTG), precentral gyrus, cerebellum lobule IV/V. Negative trends were observed in the BNST (z = -2.431), left temporal pole (z = -3.6275), right thalamus (z = -3.2568), and cerebellum IX (z = -3.2954). Positive correlations were identified in the right DLPFC, right temporal pole, fusiform gyrus, inferior temporal gyrus (ITG), superior temporal gyrus (STG), cuneus, and occipital gyri. In HC, positive correlations were identified in the BNST, locus coeruleus, right insula, and septal nuclei (z = 2.399). Between-group comparisons of these correlations were not performed.

3.8. BNST task-based functional co-occurrence

Group level tbFC of the BNST (Jennings et al., 2013; LeDoux and Pine, 2016; Pitman et al., 2012) in the trauma versus neutral word contrast was calculated as described in the Methods section. We observed accentuated tbFC of the BNST to regions of the brain involved in the processing of negative emotions and stress, including the dmFP, dACG, PCG, amygdala, MD thalamus, striatum, hypothalamus, and septal nuclei in PTSD. Fig. 4 displays this connectivity in both PTSD and HC, in comparison to known structural and resting state functional connectivity (rsFC) of the BNST. Detailed results with associated coordinates and statistics are summarized in Supplementary Table 4.

4. Discussion

4.1. The BNST modulates the processing of trauma-related words in PTSD

The BNST is rapidly emerging as an important modulator of anxiety and the stress response. Anatomical studies in animals have revealed that the BNST is extensively linked with subcortical and limbic areas (Lebow and Chen, 2016), and electrophysiological and optogenetic studies have demonstrated that these links play a crucial role in the behavioral responses of animals to stress (Henckens et al., 2017; Asok et al., 2018; Kim et al., 2013; Steudte-Schmiedgen et al., 2016; Adam et al., 2017). The role of the BNST in PTSD is less well-established. In the present work, we used an emotional word paradigm to investigate the role of the BNST in trauma-related emotion processing in PTSD. In this paradigm, trauma-related words are used to provoke a negatively valenced emotional response, which we found to be accentuated in PTSD when compared to HC (supplementary results). We observed that the BNST was recruited in PTSD subjects in the trauma vs. neutral word condition, a finding that was not present in HC (Fig. 1D and Table 1). Activity in the BNST was present in the between group analysis and also positively correlated with symptom severity (Fig. 2B), strengthening

Table 1

Comprehensive summary of BOLD-fMRI results including within-group, between-group, and correlational analyses of the trauma versus neutral word contrast.

PTSD Word vs Neutral Word		Within-Group						Within-Group						Between-Group Comparison						Within-Group Correlation with Total CAPS Score					
Brain Regions	**BA**	**x**	**y**	**z**	**z-score**	**$p_{corrected}$**	**cluster size (mm^3)**	**x**	**y**	**z**	**z-score**	**$p_{corrected}$**	**cluster size (mm^3)**	**x**	**y**	**z**	**z-score**	**$p_{corrected}$**	**cluster size (mm^3)**	**x**	**y**	**z**	**z-score**	**$p_{corrected}$**	**cluster size (mm^3)**
BNST		-6	3	3	2.6490	[0.037]	in hCaudate cluster	-6	3	3	*-0.7282*			-6	3	3	2.6010	[0.048]	in hCaudate cluster	-6	3	3	*1.5846*		
BNST		9	6	0	3.3070	[0.006]	in hCaudate cluster	9	6	0	*-0.0997*			9	6	0	*1.9857*			9	6	0	*2.4170*	*[0.057]*	162
Septal Nuclei		0	6	6	3.0450	[0.011]	in hCaudate cluster	3	6	3	*-1.3605*			3	6	3	*2.4140*	*[0.059]*	in hCaudate cluster	3	6	3	*1.0747*		
L Habenula		-3	-24	3	3.0120	[0.007]	in hCaudate cluster	-3	-24	3	*1.6575*			-3	-24	3	*0.4188*			-3	-24	3	*-0.0856*		
R Hypothalamus		6	-9	-9	3.1674	[0.019]	in hCaudate cluster	6	-9	-9	*-1.0663*			6	-9	-9	*2.0672*			6	-9	-9	*0.4785*		
SC/MRF		-3	-30	-3	4.6996	0.0012	in hCaudate cluster	-6	-33	-6	*-0.6963*			-6	-30	-3	*2.4320*			-6	-33	-6	*0.1425*		
PAG		0	-30	-6	4.3520	[<0.001]	in hCaudate cluster	0	-30	-6	*0.4602*			0	-30	-6	*1.5787*			0	-30	-6	*0.1193*		
VTA		0	-21	-15	4.0650	[<0.001]	in hCaudate cluster	0	-21	-15	*1.1390*			0	-21	-15	*0.8034*			0	-21	-15	*0.4818*		
PPN		-3	-27	-18	3.2950	[0.008]	in hCaudate cluster	-9	-30	-21	*-0.8427*			-9	-30	-21	*0.8661*			-9	-30	-21	*2.5445*		162
LC		3	-36	-24	*2.3380*	*[0.085]*	in hCaudate cluster	3	-36	-24	*0.2594*			3	-36	-24	*0.5493*			3	-36	-24	*0.3688*		
L MFG (dlPFC)	46	-45	60	27	*-2.4380*		189	-42	54	36	*1.6778*			-42	54	36	*-2.8547*		297	-42	54	36	*1.4444*		
R MFG (dlPFC)	46	33	33	27	*-0.5798*			33	33	27	*0.9983*			33	33	27	*-0.6605*			33	33	27	*-2.9040*		2188
R MFG (dlPFC)	46	48	66	21	*-0.9299*			48	66	21	*2.1385*			48	66	21	*-3.3637*		1404	48	66	21	*-1.6699*		
L IFGoperc (Broca's)	45	-57	24	15	4.4964	0.0027	59346	-51	18	18	*3.3195*		in L IFGtriang (Broca's) cluster	-51	21	18	*0.8228*			-54	15	12	*2.4610*		243
L IFGtriang (Broca's)	45	-48	24	0	4.5630		in L IFGoperc (Broca's) cluster	-42	30	0	5.4540	<0.0001	20925	-45	27	6	*-2.7449*		243	-51	15	0	*2.7720*		162
R IFGtriang (Broca's homolog)	45	45	27	6	4.2945	0.006	9720	51	24	0	*2.8851*		in R ORBinf (lateral OFC) cluster	51	30	9	*2.7850*		324	51	30	12	*2.6996*		432
L ORBinf (lateral OFC)	47	-51	36	-9	5.0169	0.0003	in L IFGoperc (Broca's) cluster	-42	33	-3	4.8710	<0.001	in L IFGtriang (Broca's) cluster	-51	36	-9	*0.2182*			-51	36	-9	*0.0595*		
L ORBinf (lateral OFC)	47	-30	27	-21	3.8718	0.0268	in L IFGoperc (Broca's) cluster	-45	33	-18	*3.3559*		in L IFGtriang (Broca's) cluster	-30	27	-21	*1.3919*			-30	27	-21	*0.4169*		
R ORBinf (lateral OFC)	47	48	30	-9	3.6549		in R IFGtriang (Broca's homolog)	45	33	-9	*3.4980*		5913	48	30	-9	*0.7464*			48	30	-9	*0.5889*		
SFGmed (dmFP)	9	-9	42	48	4.1328	0.0109	in SFGmed (vmFP) cluster	-6	54	36	*3.2790*		2889	-3	36	45	*2.5724*		324	-9	42	48	*0.3722*		
SFGmed (vmFP)	10	-12	54	18	4.9120	<0.001	61425	15	60	9	*-3.2528*		in ORBsupmed (vmFP) cluster	-6	51	15	4.1732	0.0094	18981	-6	51	15	*0.2103*		
ORBsupmed (vmFP)	10	-9	66	6	3.4120		in SFGmed (vmFP) cluster	9	57	-3	-4.7413	0.001	30267	-6	57	0	3.7165	0.0442	in SFGmed (vmFP) cluster	-6	57	0	*-0.5931*		
L Rectus (medial OFC)	11	-12	39	-15	*-0.7607*			-12	39	-15	*-1.8840*			-12	39	-15	*-0.0392*			-12	39	-15	*-2.8172*		459
R Rectus (medial OFC)	11	12	42	-21	*-0.5644*			12	42	-21	*-0.5170*			12	42	-21	*-0.3929*			12	42	-21	*-2.7436*		162
dACG	32	-12	54	21	5.0807	0.0002	in SFGmed (vmFP) cluster	12	36	9	*-3.3699*		in ORBsupmed (vmFP) cluster	12	48	9	3.8522	0.0286	in SFGmed (vmFP) cluster	12	48	9	*0.3795*		
dACG	32	3	24	27	*0.5763*			15	30	24	*-3.3500*		in ORBsupmed (vmFP) cluster	3	24	27	*0.5236*			3	24	27	*3.2533*		1350
L PCG/CUN	23	0	-45	27	3.9051	0.024	9234	-21	-57	30	*-3.0445*		11448	-9	-51	33	3.4249	[0.012]	5589	-9	-51	33	*0.7547*		
L Hippocampus	20	-30	-12	-12	*2.7550*		in hCaudate cluster	-30	-12	-12	*0.4008*			-30	-12	-12	*0.8186*			-36	-15	-18	3.7158	0.0443	3213
L PHG	37	-33	-42	-3	*-2.6763*		2916	-27	-36	-6	-4.4143	0.0038	6156	-27	-36	-6	*1.3493*			-27	-36	-6	*-0.6011*		
R PHG	37	24	-33	-6	*-0.8520*			24	-33	-6	*-3.2299*		1458	24	-33	-6	*1.3248*			24	-33	-6	*-1.5264*		
L Amygdala	34	-24	-6	-15	3.1156	[0.012]	in hCaudate cluster	-24	-6	-15	*0.9919*			-24	-6	-15	*-0.2223*			-27	-3	-18	3.2808	[0.017]	in L Hippocampus cluster
R Amygdala	34	21	0	-18	*1.1046*			24	3	-12	*2.3690*			21	0	-18	*0.2233*			21	0	-18	3.5240	[0.009]	1917
L PoCG	43	-66	3	15	-3.8134			-66	3	15	*0.7401*			-66	3	15	-3.2128		in L STG (Wernicke's) cluster	-66	3	15	*-0.1730*		
L IPL	40	-45	-36	42	-5.2537	<0.0001	in L STG (Wernicke's) cluster	-45	-30	36	*-2.6840*			-45	-36	42	*-1.8942*			-45	-36	42	*-0.3025*		
L ANG	39	-45	-69	48	4.3062	0.0057	in L IFGoperc (Broca's) cluster	-42	-69	45	*-0.5832*			-42	-69	45	*3.0751*		1809	-42	-69	45	*0.0661*		
hCaudate		-9	15	0	4.2144	0.0081	31644	-9	24	0	*-2.4260*			-9	18	0	4.8077	0.0007	4131	-6	18	0	*2.7560*		648
L Putamen		-15	9	6	3.8768	0.0264	in hCaudate cluster	-15	9	6	*-0.2425*			-15	9	6	*2.2076*			-15	9	6	*0.8727*		
L Pallidum (GPe)		-18	-3	-9	3.7788	0.0363	in hCaudate cluster	-18	-3	-9	*1.2864*			-18	-3	-9	*0.2960*			-18	-3	-9	*1.1932*		
R Pallidum (GPe)		12	0	-6	4.1315	0.0109	in hCaudate cluster	12	0	-6	*0.5400*			12	0	-6	*2.1388*			12	0	-6	*0.4691*		
L Thalamus MD		-3	-12	12	4.0720	0.0135	in hCaudate cluster	-3	-18	6	*2.8209*		540	-3	-18	15	*2.5898*		1242	-3	-18	15	*-0.2684*		
L Thalamus VA		-6	-3	9	4.5618	0.0021	in hCaudate cluster	-6	-3	9	*0.0340*			-6	-3	9	*2.2166*			-6	-3	9	*0.5036*		
R Thalamus MD		3	-15	12	3.4810	[0.018]	in hCaudate cluster	3	-24	6	*2.7417*		in L Thalamus cluster	3	-15	12	*2.3420*		in L Thalamus MD cluster	3	-18	9	*-0.1921*		
L STG (Wernicke's)	40	-63	-21	18	-4.9844	0.0003	110565	-54	-24	30	*-2.6163*		1458	-63	-24	15	*-2.8348*		3375	-63	-24	15	*-1.1711*		
R STG (TPJ)	41	48	-24	18	-4.4660		68472	48	-27	0	4.2323	0.0076	in R MTG cluster	48	-27	12	*-3.1213*		1755	48	-27	12	*-1.1224*		
R TPOsup	38	63	6	0	-4.4980			63	9	0	*1.9328*			63	9	0	-3.3984	[0.042]	1134	63	9	0	*0.7101*		
L MTG	22	-69	-27	9	*-2.9830*			-60	-33	0	4.7621	0.0009	7263	-69	-24	6	*-2.5667*		in L STG (Wernicke's) cluster	-69	-24	6	*-0.3024*		
R MTG	21	54	-27	-3	*0.5484*			60	-30	0	4.2753	0.0064	3996	54	-27	-3	*-2.7530*		in R STG (TPJ) cluster	54	-27	-3	*0.5538*		
R ITG	20	48	6	-30	4.3485	0.0049	7641	54	6	-36	*-2.0523*			54	6	-36	*2.9219*		351	54	6	-36	*0.0436*		
L Cerebellum Crus I		-45	-63	-30	4.0067	0.017	3456	-24	-84	-30	*3.3861*		3672	-45	-63	-30	*1.4166*			-45	-63	-30	*-0.4404*		
R Cerebellum Crus I		51	-63	-33	4.2927	0.006	35235	66	-60	-36	4.4646	0.0031	1026	48	-66	-36	3.7027	0.0461	945	48	-66	-36	*1.4210*		
L Cerebellum Crus II		-51	-48	-45	*-0.5501*			-51	-45	-45	-4.2276	0.0077	2079	-51	-48	-45	*3.3653*		567	-51	-48	-45	*0.7802*		
R Cerebellum Crus II		42	-81	-36	5.1470	0.0002	in L Cerebellum Crus II cluster	42	-81	-36	-4.4067	0.0031	1203	42	-81	-36	-3.4657		1215	42	-81	-36	*1.4081*		

Note: The statistical parametric maps thresholded at an initial voxel-wise p-value < 0.001, with cluster spatial extent $> 250\ mm^3$, and the p-values at the peak voxels were corrected based on family-wise error rate over the whole brain or within a ROI (ROI corrected are labeled as [ ]) at $p_{corrected} < 0.05$. Major findings are in Orange for increased activation or positive correlation, in Blue for decreased activation or negative correlation. The regions displayed above have functional relevance to the BNST and also have at least one significant result in the contrasts shown. All subpar peaks have their z-scores listed in italic font, for showing the direction/ sign of the contrast of interest (at least 1 SD, otherwise in Pale Gray): Pale Orange for increased activation or positive correlation, Pale Blue for decreased activation or negative correlation.

Abbreviation: BNST = Bed Nucleus of the Stria Terminalis; SC = Superior Colliculus; MRF = Medial Reticular Formation; PAG = Periaqueductal Gray; VTA = Ventral Tegmental Area; LC = Locus Coeruleus; MFG = Middle Frontal Gyrus; dlPFC = Dorsal Lateral Prefrontal Cortex; IFGoperc = Opercular Part of Inferior Frontal Gyrus; IFGtriang = Triangular Part of Inferior Frontal Gyrus; ORBinf = Orbital Part of Inferior Frontal Gyrus; OFC = Orbital Frontal Cortex; SFGmed = Medial Part of Superior Frontal Gyrus; ORBsupmed = Medial Orbital Part of Superior Frontal Gyrus; dmFP = Dorsal Medial Frontal Pole; vmFp = Ventral Medial Frontal Pole; PoCG = Postcentral Gyrus; IPL = Inferior Parietal Lobule; ANG = Angular Gyrus; hCaudate = Head of Caudate; Gpe = External Globus Pallidus; MD = Medial Dorsal Nucleus; VA = Ventral Anterior Nucleus; STG = Superior Temporal Gyrus; TPJ = Temporoparietal Junction; TPOsup = Superior Part of Temporal Pole; MTG = Middle Temporal Gyrus; ITG = Inferior Temporal Gyrus.

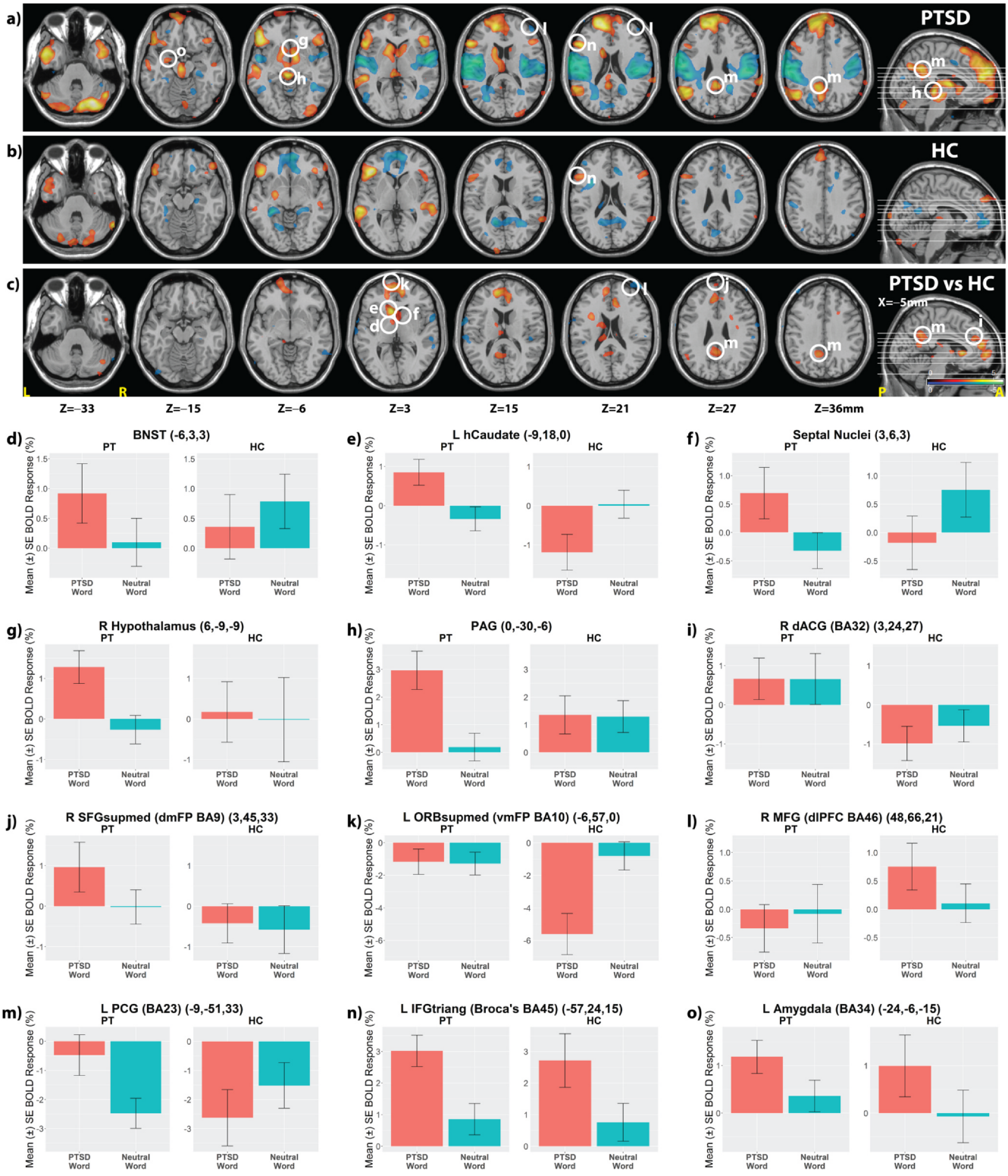

Fig. 1. Task-based BOLD fMRI of PTSD patients and healthy controls (HC) during a trauma-relevant emotional word paradigm. Panels a-c show areas of BOLD activation in the trauma word vs neutral word contrast within the patient group (a), HC (b), and in the between-group contrast (c), with statistical parametric maps thresholded at a voxel-wise $p < 0.01$ (see table 1 for whole brain or ROI corrections). Slices are selected to highlight the activity in the brainstem and cerebellum (Z = –33, −15 mm); OFC, amygdala, and hippocampus (Z = -15 mm); hypothalamus, BNST, septal nuclei, medial thalamus, and ventral striatum (Z = -6, 3, 15 mm); ventral (Z = -15 mm) and dorsal (Z = 21, 27, 36 mm) frontal poles; dACG (Z = 3, 15, 21, 27 mm); DLPFC (Z = 21 mm); and PCG (Z = 27, 36 mm). Panels (d-o) show the mean within-group BOLD response +/- standard error of the mean in select ROIs, for both PTSD patients and HC, in the trauma word and neutral word conditions. Highlighted results are shown in Table 1 and full results are shown in Supplemental Table 1.

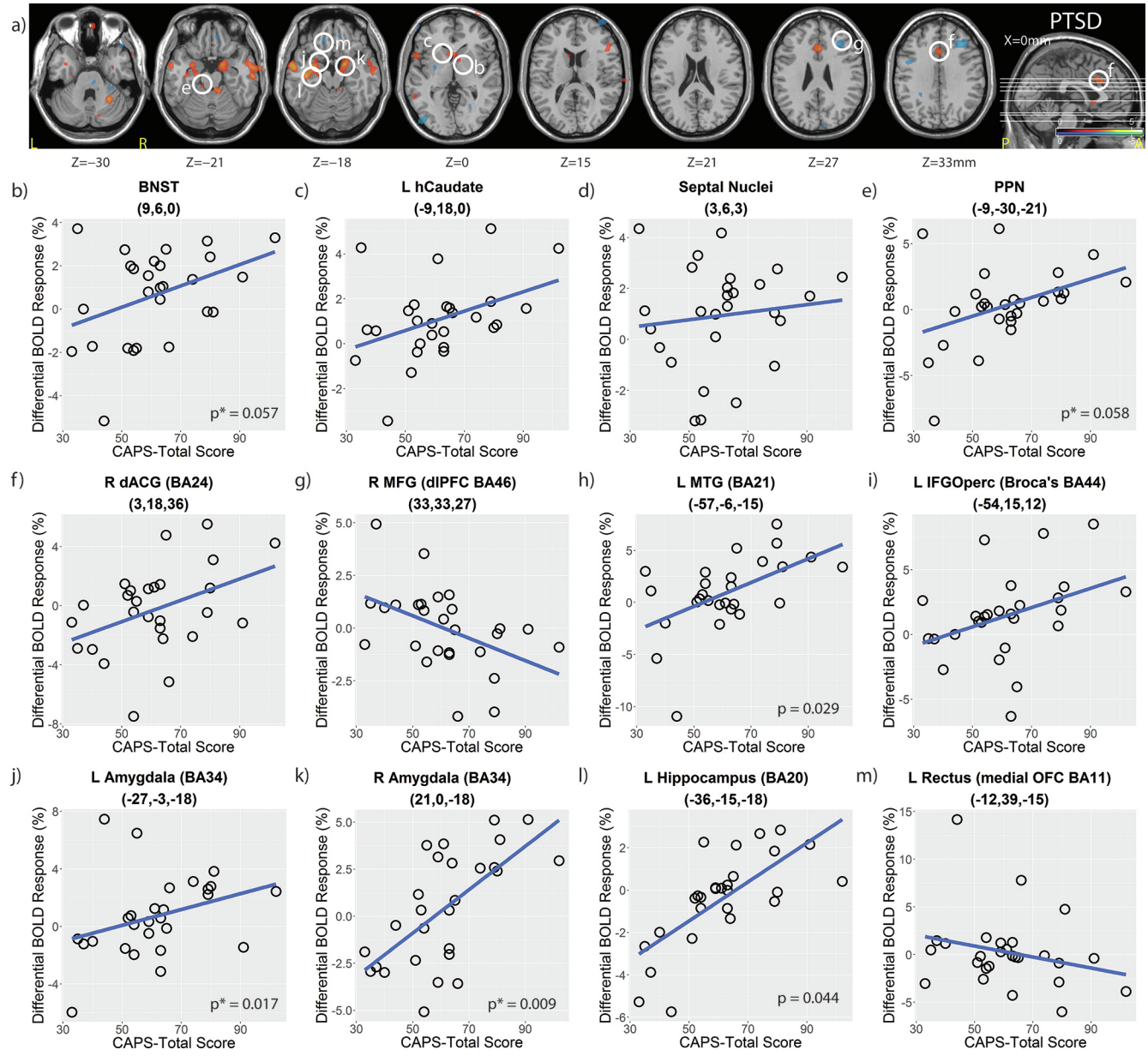

Fig. 2. Correlation of task-based BOLD activity with PTSD symptom severity. Panel (a) shows areas of positive and negative correlations at the $p < 0.01$ level of BOLD activity to PTSD symptom severity (total CAPS score) in the trauma word vs neutral word contrast within the patient group. Notable positive correlations are observed in the BNST (b), caudate head (c), septal nuclei (d), brainstem in the area of the PPN/Raphe (e), dACG in BA24 (f), left MTG in BA21 (h), Broca's area (i), amygdala (j-k), and hippocampus (l). Notable negative correlations are observed in right DLPFC (g) and left rectus in the mOFC (m). p values are displayed for correlations that surpass or are near the $p < 0.05$ threshold for statistical significance; an asterisk denotes use of ROI correction. Highlighted results are shown in Table 1 and full results are shown in Supplementary Table 2.

the implication that it plays an important role in PTSD-related emotion processing.

We also examined the relationship of the DCAI to BNST activity in the trauma vs. neutral word contrast. Previous research has shown that the BNST modulates the HPA axis via both excitatory and inhibitory projections to the hypothalamus. Excitatory projections originate in the anterior BNST and serve to activate the HPA axis in times of stress, whereas inhibitory projections originate in the posterior BNST, attenuate the stress response, and potentially protect against the development of posttraumatic behavioral changes (Lebow and Chen, 2016; Elharrar et al., 2013; Henckens et al., 2017; Lebow et al., 2012). In PTSD, chronic stress and ensuing chronically elevated cortisol levels are thought to lead to a desensitization of the HPA axis and an eventual pathological attenuation of the normal diurnal cortisol rhythm (Speer et al., 2019; Lehrner et al., 2016). However, it must be noted that studies of cortisol levels and diurnal cortisol variation in PTSD have produced mixed results (Radley et al., 2009; Radley and Johnson, 2018), so current models of HPA axis dysfunction in PTSD must be interpreted judiciously. We observed a negative correlation of BNST activity with the DCAI in PTSD and a positive correlation in HC (Fig. 3C), indicating that the BNST may be promoting a stress response and/or that the protective function of the BNST in modulating the stress response is dysfunctional in PTSD. Taken together with the BNST hyperactivity and positive correlation with symptom severity, our results fit a model in which an overactive BNST contributes to dysfunctional HPA-axis activity in PTSD. Given the overall pattern of activity described here, our findings suggest that excitatory BNST output, possibly originating in the anterior BNST, may be driving these effects. At higher

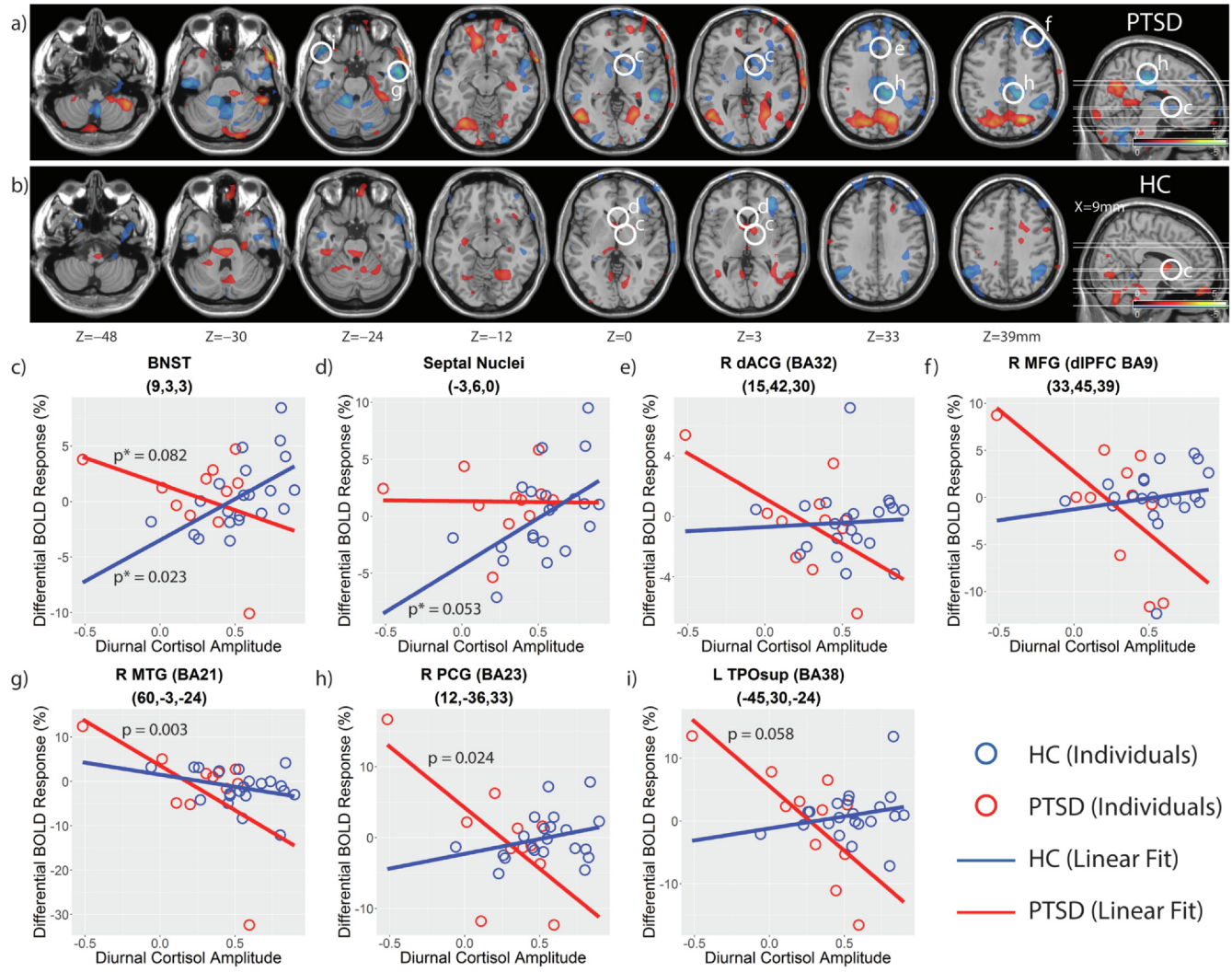

Fig. 3. Correlation of task-based BOLD activity to diurnal cortisol amplitude. Salivary cortisol measurements were taken on a non-scanning day and diurnal cortisol amplitude was calculated as described in the Methods section. Panels (a-b) shows correlations of diurnal cortisol amplitude to BOLD activity in the trauma versus neutral word contrast during the first half epoch of the emotional word paradigm. Results are displayed for PTSD patients (a) and healthy controls (b) at the $p = 0.05$ level. Negative correlations indicate that increased BOLD activity is associated with decreased diurnal cortisol amplitude, which is indicative of HPA axis pathology. PTSD patients and healthy controls demonstrated subjective differences in correlations between BOLD activity and the diurnal cortisol amplitude in the BNST (c), septal nuclei (d), right dACG (e), right DLPFC (f), right MTG in BA21 (g), right PCG (h), and left temporal pole (i). Between-group comparisons of these correlations were not performed. p values are displayed for correlations that surpass or are near the $p < 0.05$ threshold for statistical significance; an asterisk denotes use of ROI correction. Full results are shown in Supplementary Table 3.

imaging resolutions, it may be feasible to elucidate the contributions of BNST subnuclei to HPA-axis dysfunction in PTSD.

In a multivariate analysis of BNST task-based functional co-occurrence in the trauma vs. neutral word contrast, we found several differences between PTSD patients and HC (Fig. 4 and SI Table 4). In patients, there was more extensive positive tbFC between the BNST and subcortical areas (limbic striatum, hypothalamus, medial thalamus), the limbic system (amygdala and dACG), the dmFP, and cerebellar regions thought to be involved in language and emotion processing (IX and X, respectively). In HC, there was more extensive tbFC between the BNST and neocortical areas, including multiple regions of association cortex. Notably, this included negative tbFC between the BNST and the DLPFC, vmPFC (BA10), and ventromedial OFC (vmOFC). These results suggest that the BNST acts in concert with neocorticostriatal networks in HC, whereas in PTSD it acts in concert with limbic and subcortical networks, including the hypothalamus and striatum. In rodent studies, prelimbic cortex, homologous to human vmOFC, exerts an inhibitory influence on stress neurocircuitry via the BNST (Krüger et al., 2015; Torrisi et al., 2015). An analogous interpretation of our results is that the HPA-axis dysfunction described above is related to a loss of top-down regulation of stress circuitry via the BNST.

4.2. The caudate nucleus is functionally linked to the BNST

Outside the BNST, we observed elevated, symptom-correlated activity in the head of the caudate nucleus (CN) in between group analysis of the trauma vs neutral contrast (Fig. 1E, 2C, and Table 1). The BNST was robustly functionally linked to the CN in PTSD during trauma word processing (Fig. 4 and SI Table 4); the finding was also present, though less extensive, in HC. The CN receives input from the cerebral cortex and relays it downstream as part of a cortico-striato-thalamo-cortical (CSTC) circuit. Reentry loops within the circuit allow the striatum to play a complex, integratory, and modulatory role in which the processing of events can be selected or inhibited in a context-dependent fashion. Previous studies have demonstrated anatomic (Avery et al., 2014; Torrisi et al., 2017) and rsFC (Avery et al., 2014; Blumenfeld, 2016) between the BNST and CN, raising the possibility that BNST activity impacts the prioritization of cortical information processing via

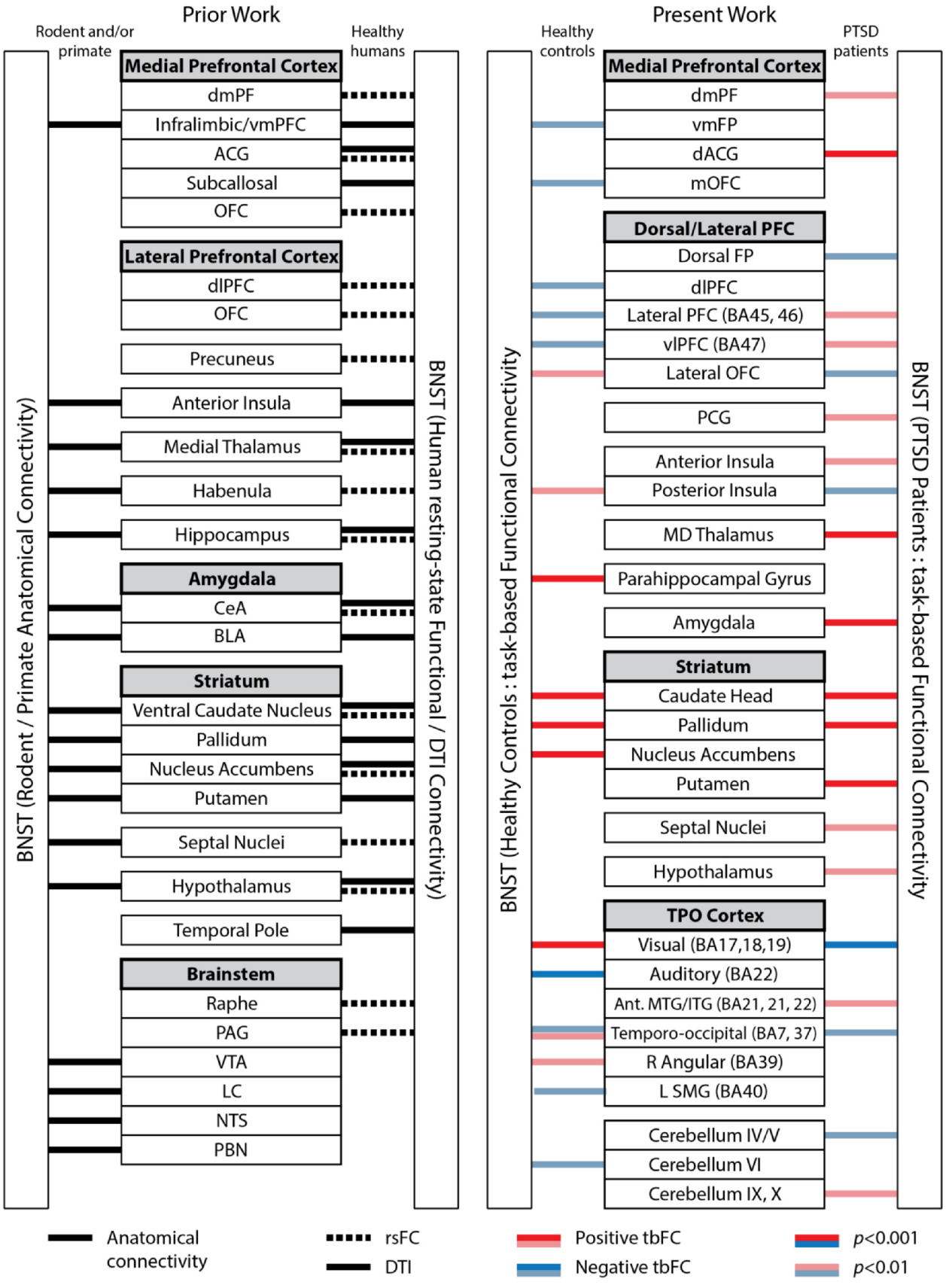

(caption on next page)

Fig. 4. Network diagram of BNST connectivity. The *left panel* summarizes BNST connectivity reported in the literature to date. Connections on the left represent anatomical connectivity discovered in tract tracing studies, primarily in rodents. Connections on the right represent healthy human structural and functional connectivity identified through DTI (solid lines) and resting-state fMRI (dotted lines), respectively. Depicted connectivity is adapted from Avery et al, Lebow et al, and Torrisi et al. The *right panel* displays task-based functional co-occurrence identified in the present study in the trauma vs neutral word contrast. Connectivity in healthy controls is shown on the left and connectivity in PTSD patients is shown on the right. Results are displayed at the $p < 0.001$ level (solid color, corresponding to $|r| > 0.5790$ for PTSD patients and $|r| > 0.6402$ for HC) and $p < 0.01$ level (pale color, corresponding to $|r| > 0.4705$ for PTSD patients and $|r| > 0.5256$ for HC). Full results are shown in Supplementary Table 4.

the CSTC. This is further supported by our observation of positive tbFC between the BNST and two additional interconnected nodes of the CTSC – the ventral pallidum and MD thalamus (Fig. 4 and SI Table 4) — in the patient group. Though animal studies have not reported anatomic connectivity between the BNST and CN, our findings add behavioral and psychiatric relevance to emerging evidence of BNST-CN FC in humans.

4.3. Stress-responsive subcortical areas co-activate with the BNST

A broader network of subcortical areas with known anatomic and rsFC to the BNST (Blumenfeld, 2016; Hikosaka, 2010) was also hyperactive in PTSD patients (Table 1), including the septal nuclei (Fig. 1F, 2D), MD and VA thalamus, hypothalamus (Fig. 1G), habenula, and brainstem (Fig. 1H, 2E). The positive effect in the septal nuclei approached statistical significance in the between-group analysis and its activity correlated both to DCAI attenuation (Fig. 3D) and BNST activity within the PTSD patient group (Fig. 4 and SI Table 4). The MD, VA, and VL nuclei of the thalamus also displayed positive tbFC with the BNST. The brainstem and thalamic nuclei participate in consciousness-supporting neural circuits through which ascending brainstem input is integrated and feedback-modulated with limbic, striatal, and neocortical information processing (Tsanov, 2017). The septum and habenula are anatomically connected to the limbic system, HPA axis, and brainstem and serve as key nodes in a stress-responsive network (Kalisch and Gerlicher, 2014; Hiser and Koenigs, 2018) that modulates arousal and action. Our results therefore implicate the BNST in a context-dependent stress response that is present in PTSD patients but not HC. The data suggest that the septal nuclei, which have little direct evidence for involvement in PTSD pathophysiology to date, contributes to this response.

4.4. Potential roles of the prefrontal cortex and lateral temporal cortex

In the prefrontal cortex, the dmPFC (including the dACG) and vmPFC were hyperactive in PTSD subjects (Fig. 1I-K), and dmPFC activity correlated positively with symptom severity (Fig. 2F) and DCAI (Fig. 3E). Conversely, HC exhibited greater activity in the right DLPFC (Fig. 1L). The mPFC has been implicated in the processing of negatively valenced information. In particular, the dmPFC and dACG co-activate during threat appraisal under low cognitive load (Kragel et al., 2018) and vmPFC activity has been associated with the generation and regulation of negative emotions (St. Jacques et al., 2011; Moser et al., 2015) and the processing of negative autobiographical information (Neumeister et al., 2017). Recruitment of these regions is increased in PTSD populations similar to those in this study (Motzkin et al., 2015; Balderston et al., 2017), and there is evidence to suggest connectivity between these regions and the BNST is an important feature of the pathophysiology of PTSD (Brinkmann et al., 2017; Raichle, 2015). In contrast, activity in the right DLPFC, a region implicated in cognitive control and less active in anxiety (Torrisi et al., 2018), was comparatively reduced in PTSD patients during the trauma vs. neutral word condition and also negatively associated with both symptom severity (Fig. 2G) and DCAI in the PTSD group (Fig. 3F). These results suggest an overall shift towards dysexecutive emotion processing in PTSD that parallels the stress response described above.

In the temporal lobes, activity in the right anterolateral temporal cortex (BA 20/21, Table 1) during the trauma vs. neutral word contrast positively correlated with symptom severity (Fig. 2H), negatively correlated with DCAI (Fig. 3G), and had positive tbFC with the BNST within the PTSD group (Fig. 4). This region is functionally connected to the default mode network (DMN) (Rabellino et al., 2018) and its activation in our study, in conjunction with activation of the mPFC (described above) and PCG (Fig. 1M, 3H), suggest increased recruitment of linguistically-driven self-referential neurocircuitry in PTSD patients during trauma word blocks (see Broca's area, Fig. 1N, 2I). The functional link between the BNST and DMN has been observed in other studies (Blumenfeld, 2016; Liberzon and Ressler, 2016; Ahrens et al., 2018) as well.

4.5. Findings in the medial temporal lobes highlight dissociation of BNST and amygdala activity

In the medial temporal lobes, activity in the hippocampus and amygdala increased to trauma-related words, but a between group effect was not present (Fig. 1O and Table 1). Activation in these regions correlated strongly to PTSD symptom severity (Fig. 2 J-L), which suggests that variance in disease severity in our patient population may account for the absence of a between-group effect. However, the amygdala was more active in the early phase of the emotional word paradigm (SI Fig. 3). Prior studies in rodents have shown that BNST activity is elevated during the response to sustained, unpredictable threat, and that an intact BNST is required for the expression of behavioral measures of sustained threat (Klumpers et al., 2017). Conversely, amygdala activity is elevated when the threat is immediate and therefore predictable. This has led to the formulation that the BNST plays an important role in maintaining a state of anxiety or apprehension in unpredictable, unsafe contexts (Lebow and Chen, 2016). Analogous findings have been demonstrated in humans both with and without PTSD. Specifically, in an auditory anticipatory threat paradigm, Hermann et al. found that BNST activity increases during a variable anticipatory period (maximum 16 sec) that occurs after the first second of cue presentation (Davis et al., 2010). Brinkmann et al. found that this effect was accentuated in PTSD (Brinkmann et al., 2017). Our results extend these findings to an emotional word context and is perhaps more relevant to daily exposures of PTSD patients. Finally, there was a positive correlation between amygdala and BNST activity in PTSD patients but not in HC (Fig. 4). The amygdala, which is central to fear learning and the pathogenesis of PTSD (Allen and Gorski, 1990) and is anatomically linked to the BNST, may therefore play a role in the recruitment of the BNST in this paradigm. Recent evidence from rodent studies supports the existence of a maladaptive, anxiogenic central nucleus of amygdala-BNST circuit (Daniel and Rainnie, 2016).

5. Limitations

There are several limitations to the present work:

- The patient and control groups were not sex-matched, yet research suggests that the BNST may differ in volume and connectivity in females and males (McEwen et al., 2015). In this study, there were too few males in the PTSD group (n = 4) for a subregroup analysis. However, because this study was not designed to examine sex differences in BNST activity, we included sex as a nuisance covariate in

the mixed-effects model in order to account for the sex-related effect. Notably, data from rodents suggests that such sex differences emerge when subjects are in the presence of the opposite sex, but this study did not involve sex-based cues, such as a male voice.
- We did not incorporate a trauma-exposed control group. Without such a group, we cannot attribute group differences observed in this study to PTSD vs. trauma exposure.
- Though trauma type was uniform across PTSD patients, there was heterogeneity in subject age and timing of trauma.
- Cortisol data was available only for a small subset of the PTSD participants (11/29); these low numbers limit the generalizability of cortisol-related results described above.
- We did not differentiate activity amongst the subnuclei of the BNST, which have distinct structural connectivity and behavioral functions; future studies utilizing ultra-high field MRI might have the potential to further differentiate these subnuclei.
- We used a probabilistic mask rather than tracing the BNST on anatomical scans. The BNST is variable in size amongst individuals, though some (Blumenfeld, 2016) have observed that these size differences become insignificant upon head size normalization.
- Patients in this study developed PTSD as a result of childhood sexual abuse; further work is necessary to generalize the findings to other types or timings of trauma.

6. Conclusion

The present work provides evidence that the BNST plays an integral role in the neurobiology of human PTSD. Previous studies have used threat-based paradigms or resting state fMRI data to implicate the BNST in PTSD (Brinkmann et al., 2017; Ahrens et al., 2018). By bringing together multiple measures, including task-based fMRI, behavioral assessments, neuroendocrine measures, and data-driven analytics, this study extends these observations and suggests a more comprehensive model of how the BNST and functionally-linked neurocircuitry contribute to PTSD. In the context of current knowledge of the BNST, our findings are consistent with a model (Fig. 5) in which BNST activity is promoted by chronic posttraumatic stress via action of brainstem arousal systems[78] and the amygdala, which project to the BNST. Chronically elevated BNST activity in atraumatic contexts contributes to activation of the HPA axis, which then becomes feedback suppressed over time (Speer et al., 2019), leading to alterations in cortical information processing[79] that are consistent with the dysexecutive processing of negative emotions. An overactive BNST may further modulate neocortical-striatal information processing by promoting negatively valenced states via connectivity with the limbic striatum.

The present study implicates the BNST and functionally linked neurocircuitry in altered emotion processing and HPA-axis function in human PTSD. The neural circuits described here may represent potential therapeutic targets for drug discovery. To successfully navigate the exploration of these targets in humans, it will be important to utilize experimental paradigms, physiological analyses, and behavioral measures that are appropriately tailored to the target and population of interest.

Disclosures

At the time of submission:

Dr. Samir Awasthi is employed full time at nference, inc. and has received compensation in the form of employee stock options; nference, inc. is unrelated to the present work. All substantive work on the present study was completed prior to the start of employment.

Dr. Hong Pan has four patents submitted: System and method for Z-shim compensated echo-planar magnetic resonance imaging (issued), Systems and methods for generating biomarkers based on multivariate classification of functional imaging and associated data (issued), Searching system for biosignature extraction and biomarker discovery, and System and method for controlling physiological noise in functional magnetic resonance imaging. Dr. Pan is a co-founder of Ceretype Neuromedicine, Inc., and received founder's shares (unrelated).

Dr. David Silbersweig is the Chairman of the Department of Psychiatry at Brigham and Women's Hospital. During the past two years he has served on the advisory board of The American Foundation for Suicide Prevention. He has received funding for travel to speak at the American Neuropsychiatric Association annual meeting in 2019. He served as a consulting editor for the Journal of Neuropsychiatry and Clinical Neurosciences and serves on the Editorial Board for the Harvard Review of Psychiatry. He has four patents submitted: System and Method for z-Shim Compensated Echo-Planar Magnetic Resonance Imaging, and Systems (issued), System and Methods for Generating Biomarkers Based on Multivariate Classification of Functional Imaging and Associated Data (issued), System and Method for a Multivariate, Automated, Systematic and/or Hierarchical Searching System for Biosignature Extraction and Biomarker Discovery via task-based fMRI Imaging spacetime data, and PhyNFI: System and Method for Physiological-Noise-Free Functional Magnetic Resonance Imaging. He has publishing royalties for the textbook, Depression in Medical Illness (McGraw-Hill, 2017). He has one current consultancy, Tilak, which doesn't conflict and is unrelated. The following consultancies are in the past: Biogen, Sanofi, Philips and Goldfinch, none of which conflict and are unrelated to the paper. Dr. Silbersweig is a founder of a startup company, Ceretype Neuromedicine, Inc. Over the past two years, he received founders shares (unrelated) and founders shares in Buoyant (no current assets, unrelated).

Dr. Emily Stern is the CEO and a Co-founder of Ceretype Neuromedicine, Inc., a spin out from Brigham and Women's Hospital, Harvard Medical School (has received founders shares; not related). The submitted work was performed while she was the Director of the Functional Neuroimaging Laboratory and the Director of Functional and Molecular Neuroimaging at Brigham and Women's Hospital. Dr. Stern has four patents submitted: System and Method for z-Shim Compensated Echo-Planar Magnetic Resonance Imaging, and Systems (issued), System and Methods for Generating Biomarkers Based on Multivariate Classification of Functional Imaging and Associated Data (issued), System and Method for a Multivariate, Automated, Systematic and/or Hierarchical Searching System for Biosignature Extraction and Biomarker Discovery via task-based fMRI Imaging Spacetime Data, and PhyNFI: System and Method for Physiological-Noise-Free Functional Magnetic Resonance Imaging. During the course of the past three years, she has served as Co-Editor of the International Journal of Imaging Systems and Technology – Neuroimaging and Brain Mapping and serves on the Editorial Board of the Journal of Neuroimaging. She has received funding for travel from the National Institutes of Health and the James S. McDonnell Foundation. She has received an honorarium from the American Academy of Physical Medicine and Rehabilitation and reimbursement for service from the National Institutes of Health. Dr. Stern has received research funding support from the DHHS Administration for Community Living, formerly the National Institute on Disability and Rehabilitation Research (NIDRR – 90DP0039-03-01), the Epilepsy Foundation, the NIH (NIMH – R01MH090291, co-investigator), Northeastern University and Blackthorn Therapeutics.

CRediT authorship contribution statement

Samir Awasthi: Writing - original draft, Writing - review & editing, Visualization. **Hong Pan:** Conceptualization, Methodology, Software, Project administration, Validation, Formal analysis, Investigation, Resources, Data curation, Writing - original draft, Writing - review & editing, Visualization, Supervision, Funding acquisition. **Joseph E. LeDoux:** Conceptualization, Writing - review & editing, Funding acquisition. **Marylene Cloitre:** Conceptualization, Investigation, Writing - review & editing. **Margaret Altemus:** Conceptualization, Resources, Writing - review & editing. **Bruce McEwen:** Conceptualization,

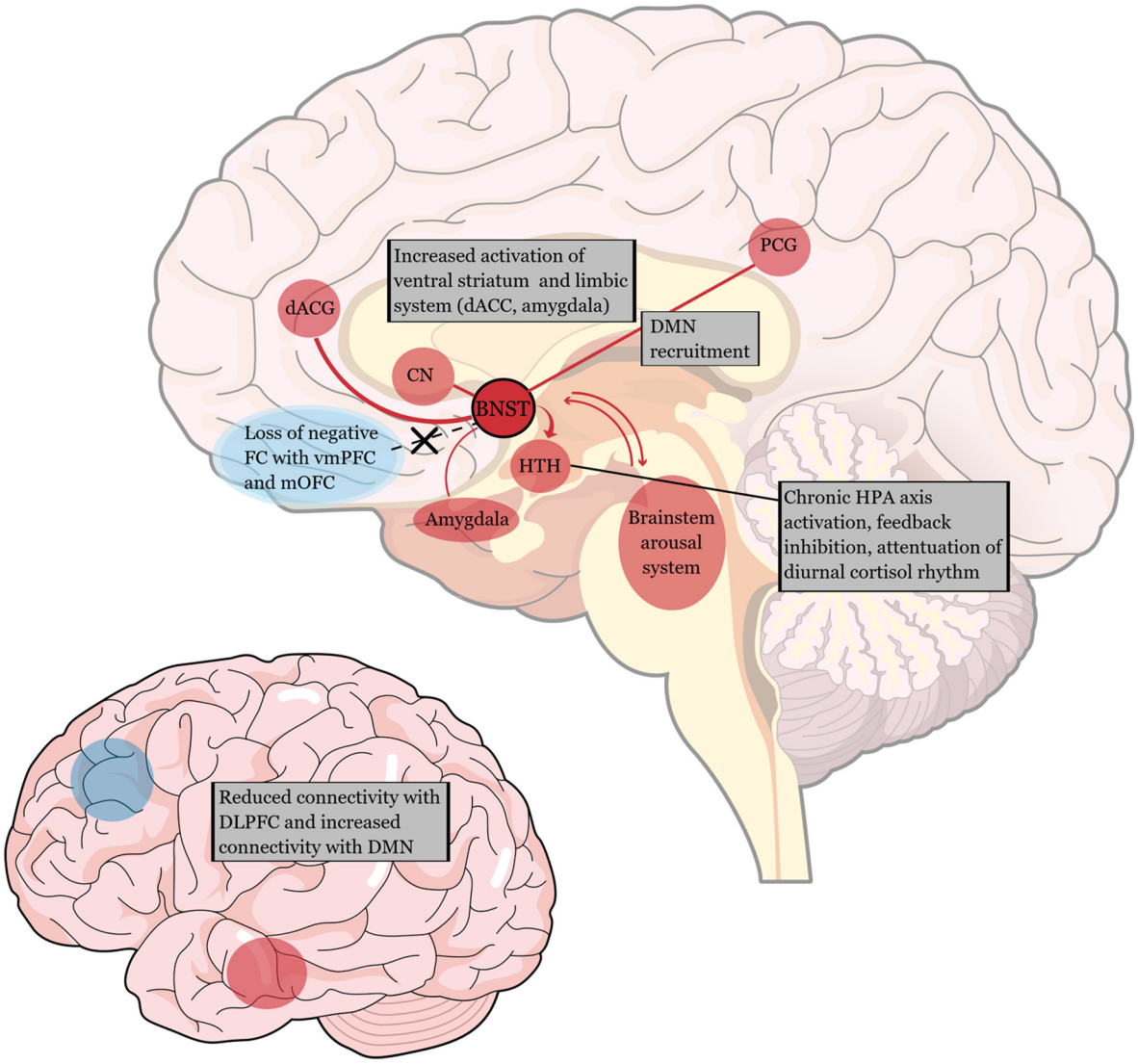

Fig. 5. Diagrammatic representation of the role of the BNST in PTSD. In this model, chronic posttraumatic stress promotes BNST activity via the amygdala and brainstem arousal networks. The BNST contributes to activation of the HPA axis, which over time becomes feedback suppressed, leading to changes in cortical information processing that are consistent with a shift towards the dysexecutive processing of negative emotions. In this model, the BNST further impacts neocortical-striatal information processing by promoting negatively valenced states via connectivity with the limbic striatum. Finally, there is a loss of functional connectivity between the BNST and dorsolateral prefrontal and ventromedial orbitofrontal cortex, which may reflect a loss of prefrontal top-down inhibitory influence that these regions exert on stress-related neurocircuitry.

Methodology, Funding acquisition. **David Silbersweig:** Conceptualization, Methodology, Resources, Writing - review & editing, Supervision, Project administration, Funding acquisition. **Emily Stern:** Conceptualization, Methodology, Resources, Writing - review & editing, Supervision, Project administration, Funding acquisition.

Declaration of Competing Interest

The authors declare that they have no known competing financial interests or personal relationships that could have appeared to influence the work reported in this paper.

Acknowledgements

Funding for this study was provided by the NIMH Grant P50 MH58911-S1.

Appendix A. Supplementary data

Supplementary data to this article can be found online at https://doi.org/10.1016/j.nicl.2020.102442.

References

Longo, D.L., Shalev, A., Liberzon, I., Marmar, C., 2017. Post-Traumatic Stress Disorder. N Engl J Med 376 (25), 2459–2469.
Ross, D.A., et al., 2017. An Integrated Neuroscience Perspective on Formulation and Treatment Planning for Posttraumatic Stress Disorder: An Educational Review. JAMA Psychiatry 74 (4), 407. https://doi.org/10.1001/jamapsychiatry.2016.3325.
Pitman, R.K., et al., 2012. Biological studies of post-traumatic stress disorder. Nat Rev Neurosci 13 (11), 769–787.
Etkin, A., Egner, T., Kalisch, R., 2011. Emotional processing in anterior cingulate and medial prefrontal cortex. Trends in Cognitive Sciences 15 (2), 85–93.
Lebow, M.A., Chen, A., 2016. Overshadowed by the amygdala: the bed nucleus of the stria terminalis emerges as key to psychiatric disorders. Mol Psychiatry 21 (4), 450–463.
LeDoux, J.E., Pine, D.S., 2016. Using Neuroscience to Help Understand Fear and Anxiety: A Two-System Framework. AJP 173 (11), 1083–1093.
Adhikari, A., 2014. Distributed circuits underlying anxiety. Front Behav Neurosci 8, 112. https://doi.org/10.3389/fnbeh.2014.00112.
Grupe, D.W., Nitschke, J.B., 2013. Uncertainty and anticipation in anxiety: an integrated

neurobiological and psychological perspective. Nat Rev Neurosci 14 (7), 488–501.
Jennings, J.H., et al., 2013. Distinct extended amygdala circuits for divergent motivational states. Nature 496 (7444), 224–228.
Elharrar, E., et al., 2013. Overexpression of Corticotropin-Releasing Factor Receptor Type 2 in the Bed Nucleus of Stria Terminalis Improves Posttraumatic Stress Disorder-like Symptoms in a Model of Incubation of Fear. Biol. Psychiatry 74 (11), 827–836.
Henckens, M.J.A.G., et al., 2017. CRF receptor type 2 neurons in the posterior bed nucleus of the stria terminalis critically contribute to stress recovery. Mol Psychiatry 22 (12), 1691–1700.
Lebow, M., et al., 2012. Susceptibility to PTSD-Like Behavior Is Mediated by Corticotropin-Releasing Factor Receptor Type 2 Levels in the Bed Nucleus of the Stria Terminalis. J. Neurosci. 32 (20), 6906–6916.
Brinkmann, L., et al., 2017. Dissociation between amygdala and bed nucleus of the stria terminalis during threat anticipation in female post-traumatic stress disorder patients: Threat Anticipation in PTSD. Hum. Brain Mapp. 38 (4), 2190–2205.
Avery, S.N., et al., 2014. BNST neurocircuitry in humans. NeuroImage 91, 311–323.
Asok, A., et al., 2018. Optogenetic silencing of a corticotropin-releasing factor pathway from the central amygdala to the bed nucleus of the stria terminalis disrupts sustained fear. Mol Psychiatry 23 (4), 914–922.
Hammack, S.E., et al., 2010. Roles for Pituitary Adenylate Cyclase-Activating Peptide (PACAP) Expression and Signaling in the Bed Nucleus of the Stria Terminalis (BNST) in Mediating the Behavioral Consequences of Chronic Stress. J Mol Neurosci 42 (3), 327–340.
Goode, T.D., Maren, S., 2017. Role of the bed nucleus of the stria terminalis in aversive learning and memory. Learn. Mem. 24 (9), 480–491.
Rodriguez-Sierra, O. E., Goswami, S., Turesson, H. K. & Pare, D. Altered responsiveness of BNST and amygdala neurons in trauma-induced anxiety. Transl Psychiatry 6, e857, doi:10.1038/tp.2016.128 (2016).
Somerville, L.H., Whalen, P.J., Kelley, W.M., 2010. Human Bed Nucleus of the Stria Terminalis Indexes Hypervigilant Threat Monitoring. Biol. Psychiatry 68 (5), 416–424.
Herrmann, M.J., et al., 2016. Phasic and sustained brain responses in the amygdala and the bed nucleus of the stria terminalis during threat anticipation: Amygdala and BNST in Phasic and Sustained Fear. Hum. Brain Mapp. 37 (3), 1091–1102.
Davis, M., Walker, D.L., Miles, L., Grillon, C., 2010. Phasic vs Sustained Fear in Rats and Humans: Role of the Extended Amygdala in Fear vs Anxiety. Neuropsychopharmacol 35 (1), 105–135.
Klumpers, F., Kroes, M.C.W., Baas, J.M.P., Fernández, G., 2017. How Human Amygdala and Bed Nucleus of the Stria Terminalis May Drive Distinct Defensive Responses. J. Neurosci. 37 (40), 9645–9656.
Weisholtz, D.S., et al., 2015. Beyond the amygdala: Linguistic threat modulates perisylvian semantic access cortices. Brain Lang. 151, 12–22.
Isenberg, N., et al., 1999. Linguistic threat activates the human amygdala. Proc. Natl. Acad. Sci. 96 (18), 10456–10459.
First, M. B. & Gibbon, M. in Comprehensive handbook of psychological assessment, Vol. 2: Personality assessment. 134-143 (John Wiley & Sons Inc, 2004).
Beck, A.T., Ward, C.H., Mendelson, M., Mock, J., Erbaugh, J., 1961. An inventory for measuring depression. Arch Gen Psychiatry 4, 561–571. https://doi.org/10.1001/archpsyc.1961.01710120031004.
Spielberger, C.D., 1983. State-Trait Anxiety Inventory for Adults (STAI-AD). APA PsycTests. https://doi.org/10.1037/t06496-000.
Wiener, A., 1992. The Dissociative Experiences Scale. Am. J. Psychiatry 149 (1), 143-a–143.
Spielberger, C.D., 1999. Sate-Trait Anger Expression Inventory-2: STAXI-2. PAR, Psychological Assessment Ressources.
Foa, E.B., Cashman, L., Jaycox, L., Perry, K., 1997. The validation of a self-report measure of posttraumatic stress disorder: The Posttraumatic Diagnostic Scale. Psychol. Assess. 9 (4), 445–451.
Carver, C.S., Scheier, M.F., Weintraub, J.K., 1989. Assessing coping strategies: A theoretically based approach. J. Pers. Soc. Psychol. 56, 267–283. https://doi.org/10.1037/0022-3514.56.2.267.
Reiss, S., Peterson, R.A., Gursky, D.M., McNally, R.J., 1986. Anxiety sensitivity, anxiety frequency and the prediction of fearfulness. Behav. Res. Ther. 24 (1), 1–8.
Blake, D.D., et al., 1995. The development of a clinician-administered PTSD scale. J. Traum. Stress 8 (1), 75–90.
Macmillan, N. A. & Creelman, D. C. Detection Theory: A User's Guide. 2 edn, (Lawrence Erlbaum Associates, Inc., 2005).
Protopopescu, X., et al., 2005. Differential time courses and specificity of amygdala activity in posttraumatic stress disorder subjects and normal control subjects. Biol. Psychiatry 57 (5), 464–473.
Gu, H., et al., 2002. Single-Shot Interleaved Z-Shim EPI with Optimized Compensation for Signal Losses due to Susceptibility-Induced Field Inhomogeneity at 3 T. NeuroImage 17 (3), 1358–1364.
Friston, K., 2007. In: Statistical Parametric Mapping. Elsevier, pp. 10–31. https://doi.org/10.1016/B978-012372560-8/50002-4.
Pan, H., Epstein, J., Silbersweig, D.A., Stern, E., 2011. New and emerging imaging techniques for mapping brain circuitry. Brain Res. Rev. 67 (1-2), 226–251.
Frank, L.R., Buxton, R.B., Wong, E.C., 2001. Estimation of respiration-induced noise fluctuations from undersampled multislice fMRI data. Magn. Reson. Med. 45 (4), 635–644.
Worsley, K.J., et al., 2002. A General Statistical Analysis for fMRI Data. NeuroImage 15 (1), 1–15.
Aguirre, G.K., Zarahn, E., D'Esposito, M., 1998. The Variability of Human, BOLD Hemodynamic Responses. NeuroImage 8 (4), 360–369.
McGonigle, D.J., et al., 2000. Variability in fMRI: An Examination of Intersession Differences. NeuroImage 11 (6), 708–734.
Theiss, J.D., Ridgewell, C., McHugo, M., Heckers, S., Blackford, J.U., 2017. Manual segmentation of the human bed nucleus of the stria terminalis using 3 T MRI. NeuroImage 146, 288–292.
Craddock, R.C., James, G.A., Holtzheimer III, P.E., Hu, X.P., Mayberg, H.S., 2012. A whole brain fMRI atlas generated via spatially constrained spectral clustering. Hum. Brain Mapp. 33 (8), 1914–1928.
Shi, J.B., Malik, J., 2000. Normalized cuts and image segmentation. IEEE Trans. Pattern Anal. Mach. Intell. 22, 888–905. https://doi.org/10.1109/34.868688.
Foley, P., Kirschbaum, C., 2010. Human hypothalamus–pituitary–adrenal axis responses to acute psychosocial stress in laboratory settings. Neurosci. Biobehav. Rev. 35 (1), 91–96.
Lovallo, W.R., Robinson, J.L., Glahn, D.C., Fox, P.T., 2010. Acute effects of hydrocortisone on the human brain: An fMRI study. Psychoneuroendocrinology 35 (1), 15–20.
Garcia-Garcia, A L, Canetta, S, Stujenske, J M, Burghardt, N S, Ansorge, M S, Dranovsky, A, Leonardo, E D, 2018. Serotonin inputs to the dorsal BNST modulate anxiety in a 5-HT1A receptor-dependent manner. Mol Psychiatry 23 (10), 1990–1997.
Kim, S.Y., et al., 2013. Diverging neural pathways assemble a behavioural state from separable features in anxiety. Nature 496 (7444), 219–223.
Steudte-Schmiedgen, S., Kirschbaum, C., Alexander, N., Stalder, T., 2016. An integrative model linking traumatization, cortisol dysregulation and posttraumatic stress disorder: Insight from recent hair cortisol findings. Neurosci. Biobehav. Rev. 69, 124–135.
Adam, E.K., Quinn, M.E., Tavernier, R., McQuillan, M.T., Dahlke, K.A., Gilbert, K.E., 2017. Diurnal cortisol slopes and mental and physical health outcomes: A systematic review and meta-analysis. Psychoneuroendocrinology 83, 25–41.
Speer, K.E., Semple, S., Naumovski, N., D'Cunha, N.M., McKune, A.J., 2019. HPA axis function and diurnal cortisol in post-traumatic stress disorder: A systematic review. Neurobiol. Stress 11, 100180. https://doi.org/10.1016/j.ynstr.2019.100180.
Lehrner, A., Daskalakis, N. & Yehuda, R. Cortisol and the Hypothalamic-Pituitary-Adrenal Axis in PTSD. 265-290, doi:10.1002/9781118356142.ch11 (2016).
Radley, J.J., Gosselink, K.L., Sawchenko, P.E., 2009. A Discrete GABAergic Relay Mediates Medial Prefrontal Cortical Inhibition of the Neuroendocrine Stress Response. J. Neurosci. 29 (22), 7330–7340.
Radley, J.J., Johnson, S.B., 2018. Anteroventral bed nuclei of the stria terminalis neurocircuitry: Towards an integration of HPA axis modulation with coping behaviors - Curt Richter Award Paper 2017. Psychoneuroendocrinology 89, 239–249.
Krüger, O., Shiozawa, T., Kreifelts, B., Scheffler, K., Ethofer, T., 2015. Three distinct fiber pathways of the bed nucleus of the stria terminalis to the amygdala and prefrontal cortex. Cortex 66, 60–68.
Torrisi, S., et al., 2015. Resting state connectivity of the bed nucleus of the stria terminalis at ultra-high field: Resting State Connectivity of BNST. Hum. Brain Mapp. 36 (10), 4076–4088.
Torrisi, S., et al., 2017. Resting state connectivity of the human habenula at ultra-high field. NeuroImage 147, 872–879.
Blumenfeld, H. in The Neurology of Consciousness (eds Steven Laureys, Giulio Tononi, & Olivia Gosseries) Ch. 1, 3-29 (Academic Press, 2016).
Hikosaka, O., 2010. The habenula: from stress evasion to value-based decision-making. Nat Rev Neurosci 11 (7), 503–513.
Tsanov, M., 2017. Differential and complementary roles of medial and lateral septum in the orchestration of limbic oscillations and signal integration. Eur J Neurosci. https://doi.org/10.1111/ejn.13746.
Kalisch, R., Gerlicher, A.M.V., 2014. Making a mountain out of a molehill: On the role of the rostral dorsal anterior cingulate and dorsomedial prefrontal cortex in conscious threat appraisal, catastrophizing, and worrying. Neurosci. Biobehav. Rev. 42, 1–8.
Hiser, J., Koenigs, M., 2018. The Multifaceted Role of the Ventromedial Prefrontal Cortex in Emotion, Decision Making, Social Cognition, and Psychopathology. Biol. Psychiatry 83 (8), 638–647.
Kragel, P.A., et al., 2018. Generalizable representations of pain, cognitive control, and negative emotion in medial frontal cortex. Nat Neurosci 21 (2), 283–289.
St. Jacques, P.L., Botzung, A., Miles, A., Rubin, D.C., 2011. Functional neuroimaging of emotionally intense autobiographical memories in post-traumatic stress disorder. J. Psychiatr. Res. 45 (5), 630–637.
Moser, D. A. et al. Violence-related PTSD and neural activation when seeing emotionally charged male-female interactions. Social Cognitive and Affective Neuroscience 10, 645-653, doi:10.1093/scan/nsu099 (2015).
Neumeister, P. et al. Interpersonal violence in posttraumatic women: brain networks triggered by trauma-related pictures. Social Cognitive and Affective Neuroscience 12, 555-568, doi:10.1093/scan/nsw165 (2017).
Motzkin, J.C., et al., 2015. Ventromedial prefrontal cortex damage alters resting blood flow to the bed nucleus of stria terminalis. Cortex 64, 281–288.
Balderston, N.L., et al., 2017. Anxiety Patients Show Reduced Working Memory Related dlPFC Activation During Safety and Threat: Research Article: Anxiety Patients Show Reduced dlPFC Activity. Depress Anxiety 34 (1), 25–36.
Raichle, M.E., 2015. The Brain's Default Mode Network. Annu. Rev. Neurosci. 38 (1), 433–447.
Torrisi, S., et al., 2018. Extended amygdala connectivity changes during sustained shock anticipation. Transl Psychiatry 8 (1). https://doi.org/10.1038/s41398-017-0074-6.
Rabellino, D., et al., 2018. Resting-state functional connectivity of the bed nucleus of the stria terminalis in post-traumatic stress disorder and its dissociative subtype. *Hum. Brain Mapp.* 39 (3), 1367–1379.
Liberzon, I., Ressler, K., 2016. Neurobiology of PTSD: From Brain to Mind. Oxford University Press.
Ahrens, S., et al., 2018. A Central Extended Amygdala Circuit That Modulates Anxiety. *J. Neurosci.* 38 (24), 5567–5583.
Allen, L.S., Gorski, R.A., 1990. Sex difference in the bed nucleus of the stria terminalis of the human brain. J. Comp. Neurol. 302 (4), 697–706.
Daniel, S.E, Rainnie, D.G, 2016. Stress Modulation of Opposing Circuits in the Bed Nucleus of the Stria Terminalis. Neuropsychopharmacol 41 (1), 103–125.
McEwen, B.S, et al., 2015. Mechanisms of stress in the brain. Nat Neurosci 18 (10), 1353–1363.